# A Gold(I) Phosphine Complex Containing a Naphthalimide Ligand Functions as a TrxR Inhibiting Antiproliferative Agent and Angiogenesis Inhibitor

**ARTICLE** *in* JOURNAL OF MEDICINAL CHEMISTRY · FEBRUARY 2009

Impact Factor: 5.45 · DOI: 10.1021/jm8012135 · Source: PubMed



**11 AUTHORS**, INCLUDING:

Ingo Ott
Technische Universität Braunschweig
**132** PUBLICATIONS **3,772** CITATIONS
SEE PROFILE

Ines J Marques
Universität Bern
**16** PUBLICATIONS **391** CITATIONS
SEE PROFILE

Christoph Bagowski
University of Greifswald
**34** PUBLICATIONS **1,165** CITATIONS
SEE PROFILE

# A Gold(I) Phosphine Complex Containing a Naphthalimide Ligand Functions as a TrxR Inhibiting Antiproliferative Agent and Angiogenesis Inhibitor

Ingo Ott,*[,†,‡] Xuhong Qian,[‡] Yufang Xu,[‡] Danielle H. W. Vlecken,[§] Ines J. Marques,[§] Dominic Kubutat,[∥] Joanna Will,[∥] William S. Sheldrick,[∥] Patrick Jesse,[⊥] Aram Prokop,[⊥] and Christoph P. Bagowski[§]

*Institute of Pharmacy, Freie Universität Berlin, Königin-Luise-Strasse 2+4, 14195 Berlin, Germany, Shanghai Key Laboratory of Chemical Biology, East China University of Science and Technology, Meilong Road 130, Shanghai 200237, China, Department of Integrative Zoology, Institute of Biology, University of Leiden, AL Leiden, The Netherlands, Lehrstuhl für Analytische Chemie, Ruhr-Universität Bochum, 44780 Bochum, Germany, and Department of Pediatric Oncology/Hematology, University Medical Center Charité Berlin, D-13353 Berlin, Germany*

*Received September 25, 2008*

The novel luminescent gold(I) complex [*N*-(*N*′,*N*′-dimethylaminoethyl)-1,8-naphthalimide-4-sulfide](triethylphosphine)gold(I) was prepared and investigated for its primary biological properties. Cell culture experiments revealed strong antiproliferative effects and induction of apoptosis via mitochondrial pathways. Biodistribution studies by fluorescence microscopy and atomic absorption spectroscopy showed the uptake into cell organelles, an accumulation in the nuclei of tumor cells, and a homogeneous distribution in zebrafish embryos. In vivo monitoring of vascularisation in developing zebrafish embryos revealed a significant antiangiogenic potency of the complex. Mechanistic experiments indicated that the inhibition of thioredoxin reductase (based on the covalent binding of a gold triethylphosphine fragment) might be involved in the pharmacodynamic behavior of this novel gold species.



## Introduction

The vast majority of todays marketed drugs are organic compounds not containing metal atoms. However, the continuing success story of the platinum anticancer drugs (e.g., cisplatin; see Figure 1) and more recently the introduction of various non-platinum agents into clinical trials (e.g., the antitumor ruthenium complex NAMI-A or the ferrocenium compound ferroquine[1] for the treatment of malaria) demonstrate that there is a considerable potential for the development of novel metallodrugs, which may offer interesting pharmacological properties based on different chemical and geometrical features compared to "organic drugs".[2−4]

Among novel non-platinum based antitumor agents, gold complexes have recently gained attention because of their strong antiproliferative effects. Furthermore, a strong inhibition of the enzyme thioredoxin reductase (TrxR[a]), which is involved in tumor cell proliferation, has been noted for many derivatives and an antimitochondrial mode of action for these complexes has been proposed.[5,6]

The lead structure for antitumor-active gold complexes is auranofin (see Scheme 1), which is characterized by its gold(I) central atom as well as a triethylphosphine and a carbohydrate ligand. The mode of action of auranofin and other related gold complexes (e.g., the chloro analogue $Et_3PAuCl$) is most likely based on a covalent interaction with disulfide reductases (such as TrxR) under loss of the ligands (for a structural study on the interaction of a gold phosphole complex with the enzyme glutathione reductase, see ref 7), indicating that the active species is the gold ion itself and the ligands are more relevant for the biodistribution and kinetic properties of the agents.

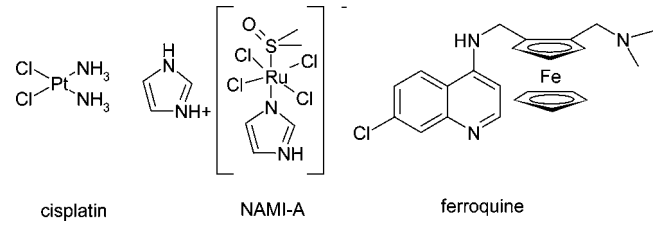


**Figure 1.** Various metallodrugs.

**Scheme 1.** Drug Development Strategy

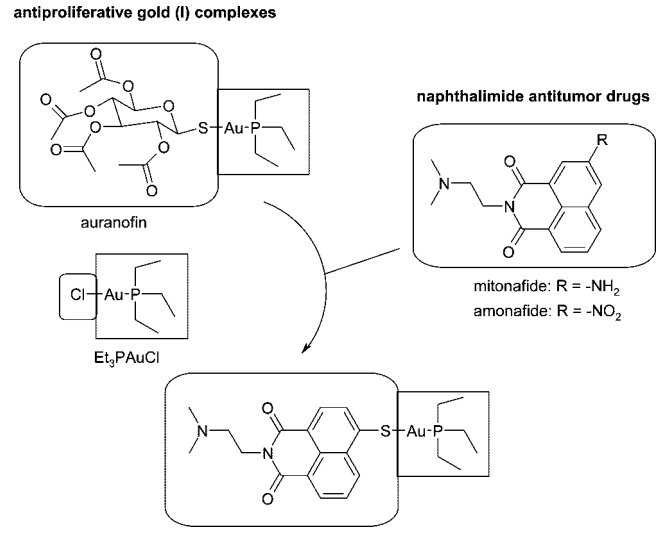


* To whom correspondence should be addressed. Address: Institute of Pharmacy, Freie Universität Berlin, Königin-Luise-Strasse 2+4, 14195 Berlin, Germany. Phone: +49 30 8385 6209. Fax: +49 8385 6906. E-mail: ottingo@zedat.fu-berlin.de.

† Freie Universität Berlin.

‡ East China University of Science and Technology.

§ University of Leiden.

∥ Ruhr-Universität Bochum.

⊥ University Medical Center Charité Berlin.

[a] Abbreviations: AAS, atomic absorption spectroscopy; DLAV, dorsal longitudinal anastomotic vessels; dpf, days postfertilization; hpf, hours postfertilization; IV, intersegmental vessels; MMP, mitochondrial membrane potential; PET, photoinduced electron transfer; SIV, subintestinal vein; TrxR, thioredoxin reductase.

10.1021/jm8012135 CCC: $40.75 
Published on Web 01/05/2009

**Scheme 2.** Synthesis of the Target Compound[a]

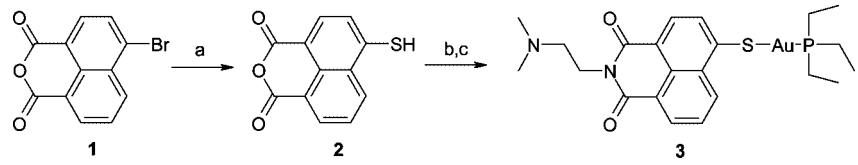


[a] (a) $Na_2S$, DMF, room temp., 6 h; (b) 2-(dimethylamino)ethylamine, EtOH, reflux heating, 6 h; (c) $Et_3PAuCl$, $CH_2Cl_2$, room temp, 5 h.

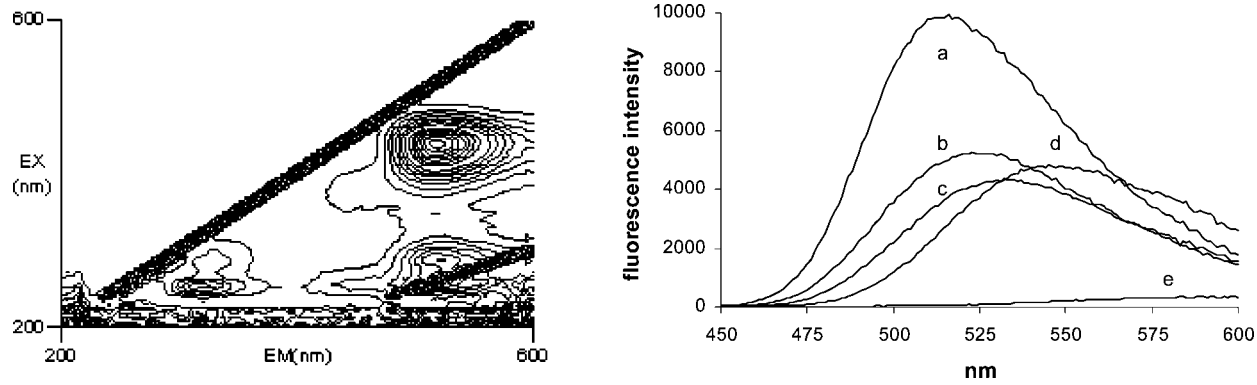


**Figure 2.** Left: 3D-contour plot of 0.5 $\mu$M **3** in $CHCl_3$. Right: emission spectra (excitation, 440 nm) of 5 $\mu$M **3** in various solvents: (a) $CHCl_3$, (b) DMF, (c) DMSO, (d) MeOH, (e) PBS.



Consequently, the nature of the ligands attached to the gold central atom is a valuable parameter for drug design. Previous structure−activity relationship studies on linear, two coordinated gold(I) complexes indicated that the presence of the phosphine ligand is important for the biological potency of the complexes, leaving the carbohydrate ligand of auranofin (or the chlorine ligand of $Et_3PAuCl$) as the first choice for structural variations.[8]

In order to create an agent with biological properties beyond those resulting from the presence of the central gold atom, the addition of an antiproliferative compound as ligand and retention of the triethylphosphine moiety were considered (as outlined in more detail in Scheme 1). We chose *N*-(*N*′,*N*′-dimethylaminoethyl)-4-mercapto-1,8-napthalimide, a ligand that contains the relevant pharmacophores of the naphthalimide class of antitumor agents: a heterocyclic naphthalimide core for DNA intercalation and a side chain containing a protonable nitrogen, which enables an initial contact to the DNA phosphate backbone.[9] As many naphthalimide derivatives exhibit interesting fluorescence properties, this ligand supposedly also provides an improved bioimaging of the compounds during in vitro and in vivo examinations. [10−17]

This report describes the preparation and primary biological evaluation of the resulting gold complex [*N*-(*N*′,*N*′-dimethylaminoethyl)-1,8-naphthalimide-4-sulfide](triethylphosphine)-gold(I).

## Chemistry

The target compound **3** was prepared by a three-step synthetic procedure (see Scheme 2). Commercially available 4-bromo-1,8-naphthalic anhydride **1** was reacted with an excess of $Na_2S$ to yield 4-mercapto-1,8-naphthalic anhydride **2**, which was converted to a naphthalimide intermediate by reflux heating with 2-(dimethylamino)ethylamine. Finally, the gold phosphine complex **3** was obtained by reaction of the crude intermediate with chloro(triethylphosphine)gold(I) and isolated by column chromatography. The structure was confirmed by $^1$H NMR, ESI, and elemental analysis.

Interesting fluorescence properties of certain naphthalimide derivates have been described in a broad range of reports. For example, the fluorescence emission intensity was found to be significantly influenced by the chemical environment concerning solvent polarity, pH value, or presence of metal ions.[10−17] Regarding metal ions, enhancement of the signal intensity was also observed depending on the nature of the respective metal. Interestingly, for gold naphthalene complexes room temperature phosphorescence from the naphthalene chromophore has been reported recently.[18] In this context it was of interest to characterize the basic fluorescence properties of **3**.

Figure 2 (left) shows a contour plot obtained with **3** in $CHCl_3$. Significant fluorescence emission was observed with a broad maximum at Ex/Em 440/516 nm. Emission spectra recorded in solvents with differing polarity (see Figure 2, right) showed that the strongest signal intensities were present in $CHCl_3$ whereas in solvents with higher polarity (such as DMSO) the emission was significantly decreased and almost disappeared in aqueous buffer solution (PBS, pH 7.4). In 1 N NaOH or 1 N HCl no emission signals could be recorded (data not shown). Besides this lowered intensity, a red shift of the maxima and broadening of the spectra were found in the more polar media compared to the measurements in $CHCl_3$ (emission maxima for excitation at 440 nm: $CHCl_3$, 514−518 nm; DMF, 521−528 nm; DMSO, 530−535 nm; MeOH, 542−546 nm).

The described effects can be attributed to an influence of the solvent polarity on the photoinduced electron transfer (PET) between the side chain nitrogen and the aromatic naphthalimide moiety. In solvents with higher polarity the PET can be hampered because of an interaction of solvent molecules with the free electron pair of the side chain nitrogen.

## Antiproliferative Effects and Biodistribution

The antiproliferative effects of **3** were evaluated in HT-29 colon carcinoma and MCF-7 breast cancer cells. As a gold phosphine containing reference, $Et_3PAuCl$ was used. $IC_{50}$ values obtained with **3** were slightly lower than those obtained with $Et_3PAuCl$ in both cell lines (HT-29 cells, 5.3 ± 1.9 $\mu$M for $Et_3PAuCl$ and 2.6 ± 0.4 $\mu$M for **3**; MCF-7 cells, 3.2 ± 1.3 $\mu$M for $Et_3PAuCl$ and 1.3 ± 0.7 $\mu$M for **3**), indicating that the replacement of the chlorine of $Et_3PAuCl$ by the naphthalimide

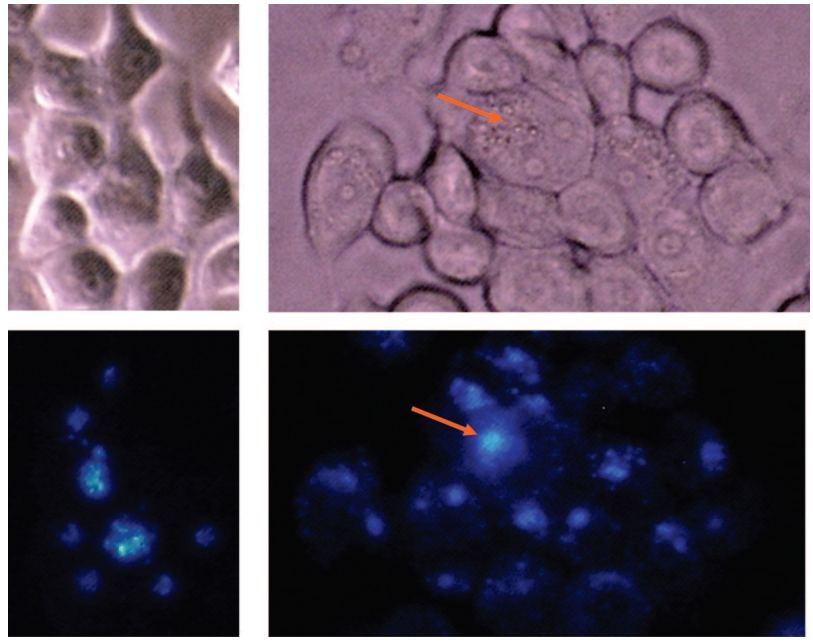

**Figure 3.** Microscopic images (40-fold enlargement) of cells incubated with 5 $\mu$M **3** for 6 h: (top left) bright-field image of HT-29 cells; (top right) bright-field image of MCF-7 cells; (bottom left) luminescence image of HT-29 cells; (bottom right) luminescence image of MCF-7 cells. For MCF-7 cells an area showing increased luminescence colocalized with morphological cell surface changes is indicated by orange arrows.



ligand (as realized in **3**) offers a suitable strategy to obtain bioactive compounds. For auranofin similar activity had been noted in the same assay during previous investigations ($IC_{50}$ values of 2.6 $\mu$M in HT-29[19] and 1.1 $\mu$M in MCF-7[20] cells).

On the basis of the above-described fluorescence characteristics, the cellular distribution of **3** could be studied by fluorescence microscopy (see Figure 3). For both HT-29 and MCF-7 cells exposed to **3**, significant blue emission was observed. Interestingly, the luminescence was not spread all over the cells and appeared to be located in specific areas within the cells. In MCF-7 cells the emission was found to be colocalized with cell surface areas showing significant morphological alterations.

Due to the mentioned effects of the solvent polarity on the fluorescence intensity (see Figure 2, right), it can be assumed that **3** is not detectable in the aqueous cytosolic parts of the cells but will show strong emission if located within the apolar membranes of cell organelles or chemical environment of medium polarity. Thus, the observed distribution of fluorescence emission can be attributed to the uptake of **3** in specific cell compartments.

In this context it is of interest to note that the biodistribution of a luminescent gold(I) N-heterocyclic carbene complex into the lysosomes has been reported recently and an enhanced uptake of various gold(I) complexes into mitochondria has been determined.[21−23]

On the basis of its low detection limits and high analytical selectivity, atomic absorption spectroscopy (AAS) provides a convenient tool for quantitative cellular biodistribution studies of metal complexes.[19,24,25] In the present study it was of interest to compare the biodistribution of $Et_3PAuCl$, which cannot be detected by fluorescence microscopy, with that of **3**.

Therefore, we isolated the nuclei of HT-29 and MCF-7 cells and investigated them for their gold content by AAS (see Table 1). After incubation with $Et_3PAuCl$ the nuclei of both cell lines contained only a small amount of gold. Upon exposure to **3** the nuclear gold concentration was increased strongly in comparison to the results obtained with $Et_3PAuCl$ (approximately 5-fold for HT-29 cells and approximately 25-fold for MCF-7 cells). The nuclear metal concentration resulting from exposure to **3** was high in comparison to other metallodrugs investigated in the same assay (e.g., up to 0.22 nmol/mg for a cobalt nucleoside derivative in MCF-7 cells[26] or certain cobalt peptide nucleic acid bioconjugates in HT-29 cells[25]). These data clearly demonstrate that the naphthalimide ligand, which itself represents a DNA targeting structure,[9] is able to transport considerable amounts of the gold phosphine moiety into the nuclei, making the DNA a reasonable biological target for **3**.

**Table 1.** Uptake into the Nuclei of Tumor Cells after 24 h of Exposure Expressed as (nmol of Gold)/(mg of Nuclear Protein)

| | HT-29 | MCF-7 |
|---|---|---|
| $Et_3PAuCl$ | 0.076 ± 0.012 | 0.052 ± 0.004 |
| **3** | 0.350 ± 0.099 | 1.399 ± 0.132 |

## Interaction with TrxR and Induction of Apoptosis

The inhibition of the enzyme thioredoxin reductase had to be considered as another potential mechanism responsible for the antiproliferative effects of **3**. Thus, the inhibitory potentials of $Et_3PAuCl$ and **3** were studied using isolated rat liver TrxR by the DTNB (dithiobisnitrobenzoic acid) reduction assay. This assay makes use of the fact that TrxR reduces the disulfide bonds of DTNB with formation of 5-thionitrobenzoic acid, which can be detected photometrically. In fact both agents inhibited the activity of the enzyme with low $EC_{50}$ values (0.14 ± 0.04 $\mu$M for $Et_3PAuCl$ and 0.27 ± 0.01 $\mu$M for **3**), confirming TrxR as a possible biological target.

As mentioned above, the mechanism of action of gold complexes is reportedly based on a covalent binding to cysteine or selenocysteine residues of the active site of TrxR. In order to evalute the possiblity of this mechanism for the gold complexes under study, we performed hyphenated LC/ESI tandem mass spectrometry experiments on the cysteine containing model peptide Ala-Gly-Cys-Val-Gly-Ala-Gly-Leu-Ile-Lys incubated with **3** or $Et_3PAuCl$ for 24 h at 37 °C.

The mass spectra for the resulting reaction mixtures both contained the molecular ion at $m/z$ = 1202 at high relative

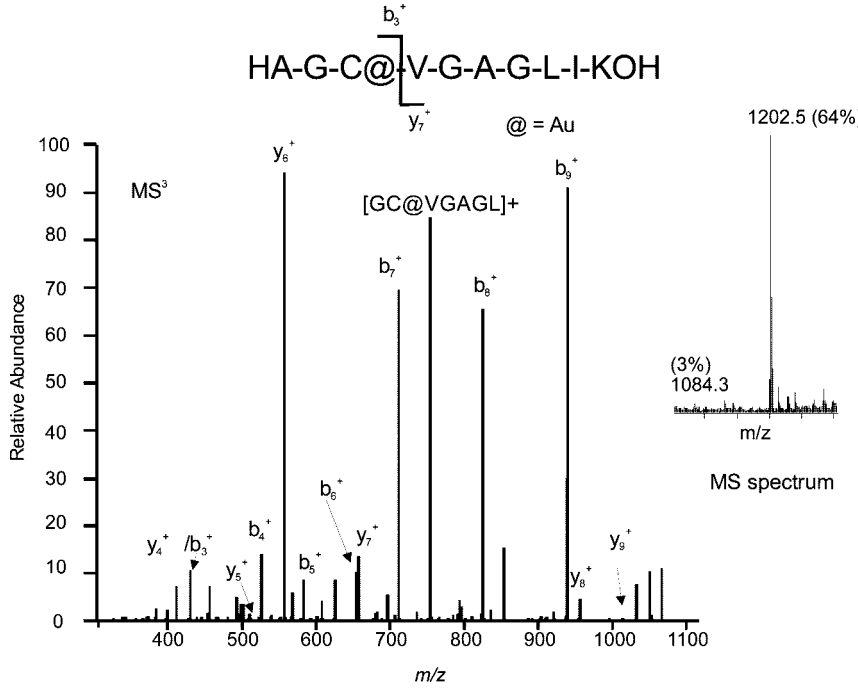


**Figure 4.** MS/MS spectrum of the molecular ion [peptide + Au]$^+$ at 1084.3 generated by neutral loss of triethylphosphine from the adduct [peptide + Au($PEt_3$)]$^+$ ($m/z$ = 1202.5).



abundance for the peptide adduct of the {($PEt_3$)Au}$^+$ fragment (see Figure 4). This indicates that a covalent binding mechanism under loss of the respective non-phosphine ligand could be relevant for both of the gold complexes. Cysteine was confirmed as the gold(I) binding site by analysis of the molecular ion at $m/z$ = 1084.3 following its formation by neutral loss of the triethylphosphine ligand from the original peptide adduct. Seven $b^+$ ions ($b_3^+$−$b_9^+$) and five $y^+$ ions ($y_5^+$−$y_9^+$) can be identified in the MS/MS spectrum of the adduct ion [peptide + Au]$^+$ (see Figure 4).

The inhibition of TrxR by gold compounds such as **3** reportedly triggers antimitochondrial and apoptotic effects.[6,23,27,28] As the investigation of these parameters makes use of assays requiring a flow cytometric analysis, which leads to less reliable results with detached adherent growing cells, suspension growing BJAB lymphoma cells were used for these studies (see Figure 5). Initially, the antiproliferative potency of **3** in these cells was confirmed (>50% reduction of cell number in concentrations between 2.5 and 10 $\mu$M; see Figure 5a).

The antiproliferative effect was accompanied by a strong induction of apoptosis (>40% DNA fragmentation; see Figure 5b) with the majority of the cells in the late stage of apoptosis (see Figure 5c). No significant necrosis was observed showing that the cell death was not caused by unspecific (physical) effects.

The measurement of the mitochondrial permeability transition reflects cells with a lower mitochondrial membrane potential (MMP) undergoing apoptosis via the mitochondrial pathway. Experiments concerning this effect showed a concentration dependent increase of cells with impaired mitochondrial permeability transition (see Figure 5d), which is in line with several reports on the antimitochondrial effects of various gold complexes.[23,27,29]

### Inhibition of Angiogenesis in Zebrafish Embryos

TrxR contributes to tumor growth and development not only by the inhibition of apoptotic events but also by the stimulation of angiogenesis.[30,31] According to this fact and motivated by reported antiangiogenic properties of other metal anticancer drugs (e.g., the ruthenium complex NAMI-A[32] or the hexacarbonyldicobalt complex Co-ASS[33]), we investigated the angiogenesis inhibiting properties of $Et_3$PAuCl and **3** by monitoring the blood vessel formation in developing zebrafish (*Danio rerio*) embryos.

Zebrafish embryos offer an established in vivo model for the study of angiogenesis and vascular development.[32−36] For the experiments we used the transgenic zebrafish line, Tg:fli1/eGFP, which exhibits a fluorescent green vasculature (based on the expression of the green fluorescence protein under an early endothelial promoter) and therefore allows microscopic live imaging of angiogenesis.[37]

The biodistribution of **3** in the embryos was evaluated 1 day after application by use of fluorescence microscopy (see Figure 6) and confirmed an efficient uptake and distribution of luminescence throughout the whole organism. At this stage of the embryo development most of the intersegmental vessels have been lumenized and possess active circulation.

We further determined for the zebrafish embryos the maximum nonlethal dose (maximum tolerated dose, MTD) for $Et_3$PAuCl and **3**. For both compounds the MTD was 0.1 $\mu$M. This concentration was the maximum dosage used for the angiogenesis experiments.

As depicted in Figure 7, treatment with **3** induced significant anti-angiogenic effects as could be observed by the impaired formation and absence of intersegmental vessels (IV), of dorsal longitudinal anastomotic vessels (DLAV), and reduced subintestinal veins (SIV) at 4 and 5 days postfertilization (dpf). Table 2 lists the details on the observed vascularisation damages. At exposure to 0.1 $\mu$M **3**, 91% of the embryos showed vessel defects. In contrast $Et_3$PAuCl induced only marginal effects on angiogenesis. Only 4% of the embryos exhibited impaired vessel formation upon treatment with 0.1 $\mu$M $Et_3$PAuCl.

The activity of **3** and the inactivity of $Et_3$PAuCl indicate that the observed angiogenesis inhibiting effects are in this case most

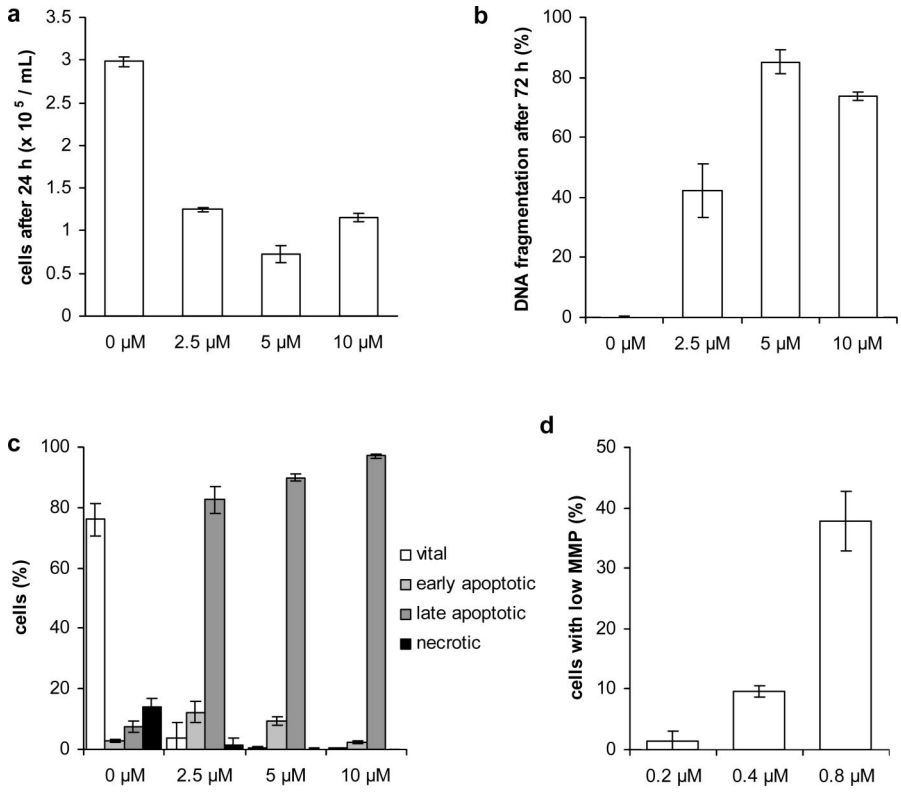


**Figure 5.** Effects of **3** in BJAB cells: (a) proliferation after 24 h: (b) DNA fragmentation after 72 h; (c) cells in apoptotic/necrotic stage after 72 h; (d) impairment of mitochondrial membrane potential (MMP) after 48 h.



probably not related to TrxR inhibition or the gold phosphine moiety and are rather a consequence of the naphthalimide ligand of **3**. Anti-angiogenic properties of naphthalimides have not been reported so far, and to the best of our knowledge **3** represents the first gold complex and the first naphthalimide for which angiogenesis inhibiting properties have been shown.

## Conclusions

The gold(I) phosphine complex **3** displayed significant antiproliferative effects in cultured tumor cells. Biodistribution experiments by fluorescence microscopy showed an efficient uptake of **3** into specific cell compartments, and AAS experiments confirmed an elevated uptake of **3** into the nuclei. As the non-naphthalimide $Et_3PAuCl$ showed a much lower nuclear uptake, it may be speculated that the naphthalimide ligand of **3** might be a useful vector to facilitate transport of metals into the nucleus. Studies on the mode of action indicated that the inhibition of TrxR and induction of apoptosis via the mitochondrial pathway also play major roles in the pharmacodynamics of this novel gold antitumor agent. For a cysteine containing model peptide the covalent binding of **3** and $Et_3PAuCl$ to the cysteine side residue after loss of the respective non-phosphine ligand could be confirmed.

Interestingly, **3** exhibited significant anti-angiogenic effects in developing zebrafish embryos in contrast to $Et_3PAuCl$, which was almost inactive in this assay. Consequently, the anti-angiogenic properties can be attributed to the naphthalimide ligand of **3**, which is not present in $Et_3PAuCl$.

The above-described results reveal a rather complex pharmacological profile of **3** and indicate the presence of multiple biological targets, of which nuclear (DNA) and mitochondrial (TrxR) macromolecules may have high relevance. The mechanism underlying the observed anti-angiogenic effects remains to be clarified.

Further studies on the pharmacodynamics and pharmacokinetics of **3** and related gold complexes are ongoing.

## Experimental Section

**General.** Chemicals and reagents were purchased from Sigma, Aldrich, or Fluka. Chloro(triethylphosphine)gold(I) ($Et_3PAuCl$) was obtained from Sigma. PBS (phosphate buffered saline), pH 7.4, was used. Compounds were freshly dissolved as stock solutions in dimethylformamide (DMF) or dimethyl sulfoxide (DMSO) prior to the experiments and diluted with the respective cell culture media or buffer during the assay procedures. Unless stated otherwise, the final concentration of the DMF or DMSO vehicle was 0.1% (V/V). NMR spectra were recorded on a 400 MHz spectrometer or a 500 MHz NMR spectrometer (Bruker). Elemental analysis was done with a Perkin-Elmer 240 C, and MS spectra were collected on an HP-1100 LC-MS spectrometer.

**Synthesis. [*N*-(*N*′,*N*′-Dimethylaminoethyl)-1,8-naphthalimide-4-sulfide](triethylphosphine)gold(I) (3).** An amount of 320 mg (1.39 mmol) of 4-mercapto-1,8-naphthalic anhydride **2** was suspended in 30 mL of absolute ethanol, and 0.55 mL (5.0 mmol) 2-(dimethylamino)ethylamine were added. The resulting mixture was slowly heated and finally kept under reflux heating for 6 h. The solvent was removed by evaporation, and the remaining dark-red oil was dried. The residue was dissolved in 25 mL of $CH_2Cl_2$, and 250 mg of chloro(triethylphosphine)gold(I) (0.71 mmol) and 0.21 g (1.52 mmol) of anhydrous $K_2CO_3$ were added. The resulting mixture was stirred at room temperature for 5 h. The solvent was evaporated and the product isolated by column chromatography (stationary phase, silica; mobile phase, $CH_2Cl_2$ and $CH_2Cl_2$/MeOH 10/1). Yield: 107 mg (0.174 mmol, 25%) of red-orange crystals. $^1$H NMR ($CDCl_3$): (ppm) 1.26 (m, 9H, $CH_3$), 1.92 (m, 6H, $CH_2$), 2.37 (s, 6H, $N(CH_3)_2$), 2.65 (t, 2H, $J = 7.2$ Hz, $CH_2$), 4.31 (t, 2H, $J = 7.2$ Hz, $CH_2$), 7.67 (dd, 1H, $J = 7.8$ Hz, $J = 8.0$ Hz, ArH6), 8.16 (d, 1H, $J = 7.8$ Hz, ArH3), 8.26 (d, 1H, $J = 7.8$ Hz, ArH2), 8.57 (m, 1H, ArH5), 9.06 (m, 1H, ArH7). HRMS: 615.15 g/mol ($M + H^+$). Anal. ($C_{22}H_{30}AuN_2O_2PS$) C, H, N.

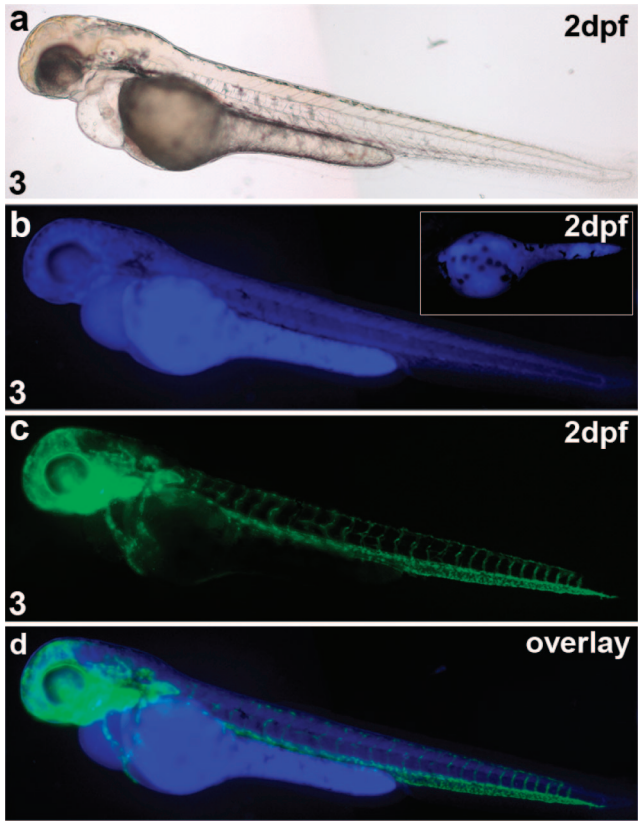


**Figure 6.** Dual contrast inverted microscopy images of zebrafish embryos exposed to 0.1 $\mu$M $Et_3PAuCl$ or 0.1 $\mu$M **3**. An example of a 2 days postfertilization (2dpf) embryo treated with 0.1 $\mu$M of **3** for 24 h is shown (a−d): (a) bright-field image; (b) luminescence image showing the blue emission of **3** (in the small window a untreated control embryo at 2dpf is depicted showing autofluorescence of the yolk but no signal in the embryo); (c) luminescence image showing the green emission of the green fluorescence protein; (d) overlay of (b) and (c).

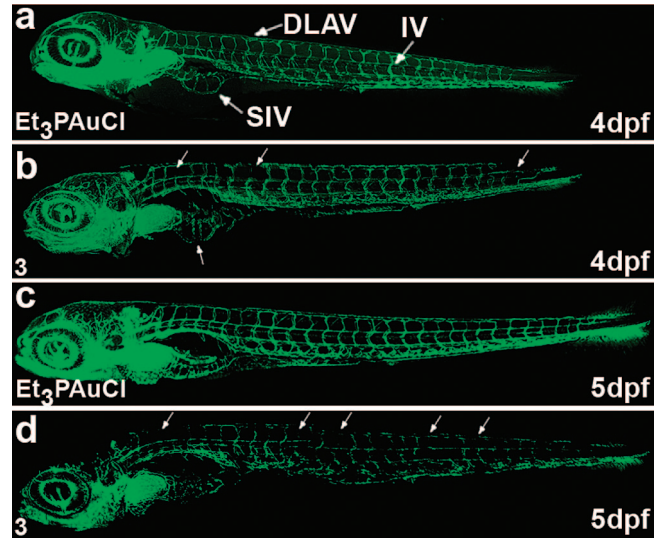


**Figure 7.** Scanning laser confocal microscopy images of zebrafish embryos exposed to $Et_3PAuCl$ (0.1 $\mu$M) or **3** (0.1 $\mu$M). Fishes were treated only once, at 1 dpf with the respective drug. Pictures show zebrafish larvae at 4 and 5 dpf, as indicated. (a) $Et_3PAuCl$ 4dpf: no vessel defects were detectable, which is similar to solvent control (DMF) treated fishes (data not shown). Examples of DLAV, IV, and SIV are marked by white arrows. b) An example of a zebrafish embryo treated with 0.1 $\mu$M **3** is shown at 4dpf. Damages of DLAV, IV, and SIV are marked with white arrows. (c) A $Et_3PAuCl$ treated embryo at 5 dpf: no vessel defects and no difference to the solvent control (DMF) treated fishes were observed (data not shown). (d) An example of a 5dpf zebrafish embryo treated with **3** shows severe damages of DLAV and IV (marked with white arrows).

**Fluorimetric Scans.** All solvents used for the fluorimetric experiments were purged with nitrogen prior to use. Compound **3** was dissolved as a stock solution (50 or 500 $\mu$M) in DMF, diluted 100-fold with the respective solvents ($CHCl_3$, DMF, DMSO, PBS, 1 N NaOH, and 1 N HCl) and measured using a Hitachi F-4500 fluorescence spectrometer. Only corrected spectra were taken.

**Antiproliferative Effects.** The antiproliferative effects in MCF-7 and HT-29 cells after 72 h (HT-29) or 96 h (MCF-7) of exposure to $Et_3PAuCl$ and **3** were evaluated according to recently described procedures.[19,20] The $IC_{50}$ value was described as that concentration reducing proliferation of untreated control cells by 50%.

**Fluorescence Microscopy of Tumor Cells.** Cells were grown in six-well plates (Sarstedt) until at least 70% confluency. The cell culture medium was replaced with fresh medium containing the compounds in a concentration of 5.0 $\mu$M (0.1% v/v DMSO) and incubated for 6 h at 37 °C in a 5% $CO_2$/95% air atmosphere. The medium was removed, and the cells were washed with PBS. Finally an amount of 500 $\mu$L of PBS was added to each well. Microscopy was performed using an Axiovert 40 CFL microscope (Zeiss) equipped with a 50 W mercury vapor short arc lamp and a Ex/Em 390 ± 11/460 ± 25 nm filter.

**Gold Content of Nuclei.** The nuclei of the tumor cells were isolated according to a described procedure with some modifications.[25,38] Cells were grown in 175 $cm^2$ cell culture flasks until at least 70% confluency. The medium was removed and replaced with 10 mL of medium containing 5.0 $\mu$M drug. After 24 h of incubation at 37 °C in a humidified atmosphere, the drug containing medium was removed, cells were trypsinized, resuspended in 10 mL of cell culture medium, and isolated by centrifugation (1500 rpm, 5 min), and 0.5−1.0 mL of 0.9% NaCl solution were added. After centrifugation (1500 rpm, 5 min) pellets were resuspended in 300 $\mu$L of RSB-1 (0.01 M Tris-HCl, 0.01 M NaCl, 1.5 mM $MgCl_2$, pH 7.4) and left for 10 min in an ice bath. The swollen cells were centrifuged (2000 rpm, 5 min), resuspended in 300 $\mu$L of RSB-2 (RSB-1 containing each 0.3% v/v Nonidet-P40 and sodium desoxycholate) and homogenized by 10−15 up/down-pushes in a 1 mL syringe with needle. The homogenate was centrifuged at 2500 rpm for 5 min, and the resulting crude nuclei were taken up in 150 $\mu$L of 0.25 M sucrose containing 3 mM $CaCl_2$. The suspension was underlayed with 150 $\mu$L of 0.88 M sucrose and centrifuged 10 min at 2500 rpm. The nuclei pellets were stored at −20 °C or immediately dissolved in 500−1000 $\mu$L of water and disrupted by use of a sonotrode. The gold content of the samples was determined by graphite furnace atomic absorption spectrometry according to a recently published procedure and the protein content by the method of Bradford.[19] Results are expressed as the mean of two independent experiments as nmol of gold per milligram of nuclear protein.

**TrxR Inhibition.** Commercially available rat liver TrxR (Sigma) was used to determine TrxR inhibition by the compounds. The assay was performed according to the manufacturer's instructions (Sigma product information sheet T9698) with appropriate modifications. Initially, the TrxR rat liver solution was diluted with potassium phosphate buffer, pH 7.0. To 25 $\mu$L aliquots of this solution (each containing approximately 0.18 units of the enyzme) each 25 $\mu$L of potassium phosphate buffer pH 7.0, containing the compounds or vehicle without compound (control) were added, and the resulting solutions were incubated for 1 h at 37 °C with moderate shaking. The solutions were transferred quantitatively to 96-well plates, and each 250 $\mu$L of reaction mixture (10 mL of reaction mixture consisted of 1.0 mL of 1.0 M potassium phosphate buffer, pH 7.0, 0.20 mL of 500 mM EDTA solution pH 7.5, 0.80 mL of 63 mM DTNB in ethanol, 0.10 mL of 20 mg/mL bovine serum albumine, 0.05 mL of 48 mM NADPH and 7.85 mL of water) were added. To correct for nonenzymatic product formation, 50 $\mu$L of 1.0 M potassium phosphate buffer, pH 7.0, and 250 $\mu$L of reaction mixture were processed simultaneously (blank value). After proper mixing

**Table 2.** Effects on Angiogenesis[a]

| compd [concn] | total embryos (with defects) [% with defects] | DLAV | DLAV + IV | DLAV + SIV | DLAV + IV + SIV |
|---|---|---|---|---|---|
| **3** [0.1 $\mu$M ] | 200 (181) [91%] | 32 | 25 | 19 | 105 |
| **3** [0.05 $\mu$M] | 200 (101) [51%] | 14 | 22 | 16 | 49 |
| $Et_3PAuCl$ [0.1 $\mu$M ] | 200 (7) [4%] | 4 | 3 | 0 | 0 |
| $Et_3PAuCl$ [0.05 $\mu$M] | 200 (4) [2%] | 3 | 1 | 0 | 0 |
| DMF | 200 (0) | 0 | 0 | 0 | 0 |

[a] Vessel defects were tested in live 4 dpf TG:fli1/eGFP fishes by confocal microscopy. Given is the total number of fishes tested versus the number of fishes with vessel defects and the percentage of fishes with vessel defects. Three independent experiments were combined with similar results. Fishes were viable and showed no significant mortality at 0.1 $\mu$M $Et_3PAuCl$ and 0.1 $\mu$M **3**, which was for both compounds the maximal tolerated dose. The solvent (DMF) was used at 0.1% v/v as control. The number of embryos with defects in the different vessels and in the combinations shown is listed. Defects only in IV or only in SIV and in the combination of both were not found.

the formation of 5-thionitrobenzol was monitored in a microplate reader (Flashscan, AnalytikJena AG) at 412 nm in 12 s intervals for 4 min. The absorbance of the blank was subtracted from that of the control and treated wells. The increase in 5-thionitrobenzol concentration over time followed a linear trend ($r^2 \geq 0.99$), and the enzymatic activities were calculated as the slopes (increase in absorbance per second) thereof. The $EC_{50}$ values were calculated as the concentration of compound decreasing the enzymatic activity of the untreated control by 50%.

**Mass Spectrometry.** ESI-MS and MS/MS spectra were collected on a Finnigan LCQ mass spectrometer (Thermo Electron Corp., San Jose, CA), which was operated in the positive ion mode with a capillary temperature of 200 °C and a spray voltage of 1.8 kV. Samples were prepared by incubating the model peptide AGCV-GAGLIK with complexes $Et_3PAuCl$ and **3** at a 1:5 molar ratio for 24 h at 37 °C. Delivery to the mass spectrometer was performed by a syringe pump operating at a flow rate of 1.0 $\mu$L/min. The relative collision energy for collision-induced dissociation was set at 30%.

**Determination of Cell Concentration and Cell Viability of BJAB Cells.** Cell viability was determined by CASY cell counter + analyzer system of Innovatis (Bielefeld, Germany). Settings were specifically defined for the requirements of the used cells. With this system the cell concentration is analyzed simultaneously in three different size ranges; cell debris, dead cells, and viable cells were determined in one measurement. Cells were seeded at a density of $1 \times 10^5$ cells/mL and treated with different concentrations of the agents; nontreated cells served as controls. After 24 h of incubation, cells were resuspended properly and 100 $\mu$L of each well were diluted in 10 mL of CASYton (ready-to-use isotonic saline solution) for an immediate automated count of the cells.

**Measurement of DNA Fragmentation.** Apoptotic cell death was determined by a modified cell cycle analysis, which detects DNA fragmentation on the single cell level as described.[39,40] BJAB cells were seeded at a density of $1 \times 10^5$ cells/mL and treated with different concentrations of **3**. After 72 h of incubation at 37 °C, cells were collected by centrifugation at 1500 rpm for 5 min, washed with PBS at 4 °C, and fixed in PBS/2% (v/v) formaldehyde on ice for 30 min. After fixation, cells were pelleted, incubated with ethanol/PBS (2:1, v/v) for 15 min, pelleted, and resuspended in PBS containing 40 $\mu$g/mL RNase A. RNA was digested for 30 min at 37 °C. Afterward cells were pelleted again and finally resuspended in PBS containing 50 $\mu$g/mL propidium iodide. Nuclear DNA fragmentation was quantified by flow cytometric determination of hypodiploid DNA. Data were collected and analyzed using a FACScan (Becton Dickinson, Heidelberg, Germany) equipped with the CELLQuest software. Data are given in % hypoploidy (subG1), which reflects the number of apoptotic cells.

**Annexin-V−Propidium Iodide Binding Assay.** Cell death was determined by staining cells with annexin-V−FITC and counterstaining with propidium iodide (PI). During apoptosis, the phospholipid phosphatidylserine is exposed to the outer leaflet of the plasma membrane.[41,42] Annexin-V−FITC then binds to phosphatidylserine leading to an increase of the fluorescence. On the other hand, PI is excluded from cells with intact membranes. PI positivity is therefore a sign of cell necrosis, whereas cells that are annexin-V−FITC positive but PI negative are generally defined as apoptotic.[43] For the annexin-V−PI assay, $1 \times 10^5$ cells were washed twice with ice-cold PBS and then resuspended in binding buffer (10 mM *N*-(2-hydroxyethyl)piperazine-*N*′-3(propanesulfonicacid) (HEPES)/NaOH (pH 7.4), 140 mM NaCl, 2.5 mM $CaCl_2$) at a concentration of $1 \times 10^5$ cells/mL. Next, 10 $\mu$L of annexin-V−FITC (BD Pharmingen, Heidelberg, Germany) and 10 $\mu$L of 50 $\mu$g/mL PI (Sigma-Aldrich, Taufkirchen, Germany) were added to the cells. Analyses were performed on a FACScan (Becton Dickinson, Heidelberg, Germany) using the CellQuest analysis software.

**Measurement of the Mitochondrial Permeability Transition.** After incubation for 48 h with different concentrations of **3**, cells were collected by centrifugation at 1500 rpm at 4 °C for 5 min. Mitochondrial permeability transition was then determined by staining cells with 5,5′,6,6′-tetrachloro-1,1′,3,3′-tetraethylbenzimidazolylcarbocyanine iodide (JC-1, Molecular Probes). Then $1 \times 10^5$ cells were resuspended in 500 $\mu$L of phenol red-free RPMI 1640 without supplements and JC-1 was added to give a final concentration of 2.5 $\mu$g/mL (38 $\mu$M). The cells were incubated for 30 min at 37 °C with moderate shaking. Control cells were likewise incubated in the absence of JC-1 dye. The cells were harvested by centrifugation at 1500 rpm at 4 °C for 5 min, washed with ice-cold PBS, and resuspended in 200 $\mu$L of PBS at 4 °C. Mitochondrial permeability transition was then quantified by flow cytometric determination of cells with decreased fluorescence, i.e., with mitochondria displaying a lower membrane potential. Data were collected and analyzed using a FACScan (Becton Dickinson, Heidelberg, Germany) equipped with the CELL Quest software. Data are given in % cells with low $\Delta\Psi_m$, which reflects the number of cells undergoing mitochondrial apoptosis.

**Animal Care.** The transgenic zebrafish (*Danio rerio*) line Tg(fli1:eGFP) was used for the angiogenesis experiments, and fishes were handled in compliance with local animal care regulations and standard protocols of The Netherlands. Fishes were kept at 28 °C in aquaria with standard day/night light cycles. Substances were administered once to dechorionated 24 hpf embryos by adding stock solutions of the compounds into the water.

**Live Imaging.** Confocal pictures were taken with the Biorad Confocal microscope 1024ES (Zeiss microscope) combined with a krypton/argon laser, or with the dual laser scanning confocal microscope Leica DM IRBE (Leica). Dual inverted contrast (DIC) microscopy pictures were taken using an Axioplan 2 microscope with an AxioCam MR5 camera (Carl Zeiss).

**Acknowledgment.** Financial support by DFG-Deutsche Forschungsgemeinschaft (Project FOR-630), BMBF−Bundesministerium für Bildung and Forschung (Project CHN 08/007), and the Portuguese Foundation for Science and Technology (Grant SFRH/BD/27262/2006) is gratefully acknowledged. We are also grateful for technical support by Heike Scheffler.

**Supporting Information Available:** Elemental analysis data of **3** and the synthetic procedure of **2**. This material is available free of charge via the Internet at http://pubs.acs.org.

## References

(1) Dive, D.; Biot, C. Ferrocene Conjugates of Chloroquine and Other Antimalarials: The Development of Ferroquine, a New Antimalarial. *ChemMedChem* **2007**, *3*, 383–391.

(2) Ott, I.; Gust, R. Non Platinum Metal Complexes as Anti-Cancer Drugs. *Arch. Pharm. Chem. Life Sci.* **2007**, *340*, 117–126.
(3) Bruijnincx, P. C. A.; Sadler, P. J. New Trends for Metal Complexes with Anticancer Activity. *Curr. Opin. Chem. Biol.* **2008**, *12*, 197–206.
(4) Hambley, T. W. Metal-Based Therapeutics. *Science* **2007**, *318*, 1392–1393.
(5) Gromer, S.; Arscott, L. D.; Williams, C. H.; Schirmer, R. H.; Becker, K. Human Placenta Thioredoxin Reductase. Isolation of the Selenoenzyme, Steady State Kinetics, and Inhibition by Therapeutic Gold Compounds. *J. Biol. Chem.* **1998**, *273*, 20096–200101.
(6) Barnard, P. J.; Berners-Price, S. J. Targeting the Mitochondrial Cell Death Pathway with Gold Compounds. *Coord. Chem. Rev.* **2007**, *251*, 1889–1902.
(7) Urig, S.; Fritz-Wolf, K.; Reau, R.; Herold-Mende, C.; Toth, K.; Davioud-Charvet, E.; Becker, K. Undressing of Phosphine Gold(I) Complexes as Irreversible Inhibitors of Human Disulfide Reductases. *Angew. Chem., Int. Ed.* **2006**, *45*, 1881–1886.
(8) Mirabelli, C. K.; Johnson, R. K.; Hill, D. T.; Faucette, L. F.; Girard, G. R.; Kuo, G. Y.; Sung, C. M.; Crooke, S. T. Correlation of the in Vitro Cytotoxic and in Vivo Antitumor Activities of Gold(I) Coordination Complexes. *J. Med. Chem.* **1986**, *29*, 218–223.
(9) Brana, M. F.; Ramos, A. Naphthalimides as Anti-Cancer Agents: Synthesis and Biological Activity. *Curr. Med. Chem.: Anti-Cancer Agents* **2001**, *1*, 237–255.
(10) Ott, I.; Xu, Y.; Liu, J.; Kokoschka, M.; Harlos, M.; Sheldrick, W. S.; Qian, X. Sulfur-Substituted Naphthalimides as Photoactivatable Anticancer Agents: DNA Interaction, Fluorescence Imaging, and Phototoxic Effects in Cultured Tumor Cells. *Bioorg. Med. Chem.* **2008**, *16*, 7107–7116.
(11) Cao, H.; Chang, V.; Hernandez, R.; Hagy, M. D. Matrix Screening of Substituted *N*-Aryl-1,8-naphthalimides Reveals New Dual Fluorescent Dyes and Unusually Bright Pyridine Derivatives. *J. Org. Chem.* **2005**, *70*, 4929–4934.
(12) Pardo, A.; Poyato, J. M. L.; Martin, E. Photophysical Properties of 1,8-Naphthalimide Derivatives. *J. Photochem.* **1987**, *36*, 323–329.
(13) Ramachandram, B.; Saroja, G.; Sankaran, N. B.; Samanta, A. Unusually High Fluorescence Enhancement of Some 1,8-Naphthalimide Derivatives Induced by Transition Metal Salts. *J. Phys. Chem. B* **2000**, *104*, 11824–11832.
(14) Zhang, Z.; Wu, D.; Guo, X.; Qian, X.; Lu, Z.; Xu, Q.; Yang, Y.; Duan, L.; He, Y.; Feng, Z. Visible Study of Mercuric Ion and Its Conjugate in Living Cells of Mammals and Plants. *Chem. Res. Toxicol.* **2005**, *18*, 1814–1820.
(15) Gan, J.; Tian, H.; Wang, Z.; Chen, K.; Hill, J.; Lane, P. A.; Rahn, M. D.; Fox, A. M.; Bradley, D. D. C. Synthesis and Luminescence Properties of Novel Ferrocene−Naphthalimides Dyads. *J. Organomet. Chem.* **2002**, *645*, 168–175.
(16) Guo, X.; Qian, X.; Jia, L. A Highly Selective and Sensitive Fluorescent Chemosensor for $Hg^{2+}$ in Neutral Buffer Aqueous Solution. *J. Am. Chem. Soc.* **2004**, *126*, 2272–2273.
(17) Xu, Z.; Qian, X.; Cui, J. Colorimetric and Ratiometric Fluorescent Chemosensor with a Large Red-Shift in Emission: Cu(II)-Only Sensing by Deprotonation of Secondary Amines as Receptor Conjugated to Naphthalimide Fluorophore. *Org. Lett.* **2005**, *7*, 3029–3032.
(18) Osawa, M.; Hoshino, M.; Hashizume, D. Photoluminescent Properties and Molecular Structures of [NaphAu($PPh_3$)] and [$\mu$-Naph{Au($PPh_3$)}$_2$]$ClO_4$ (Naph = 2-naphthyl). *Dalton Trans.* **2008**, 2248–2252.
(19) Ott, I.; Scheffler, H.; Gust, R. Development of a Method for the Quantification of the Molar Gold Concentration in Tumour Cells Exposed to Gold-Containing Drugs. *ChemMedChem* **2007**, *2*, 702–707.
(20) Ott, I.; Koch, T.; Shorafa, H.; Bai, Z.; Poeckel, D.; Steinhilber, D.; Gust, R. Synthesis, Cytotoxicity, Cellular Uptake and Influence on Eicosanoid Metabolism of Cobalt-Alkyne Modified Fructoses in Comparison to Auranofin and the Cytotoxic COX Inhibitor Co-ASS. *Org. Biomol. Chem.* **2005**, *3*, 2282–2286.
(21) Barnard, P. J.; Wedlock, L. E.; Baker, M. V.; Berners-Price, S. J.; Joyce, D. A.; Skelton, B. W.; Steer, J. H. Luminescence Studies of the Intracellular Distribution of a Dinuclear Gold(I) N-Heterocyclic Carbene. *Angew. Chem.* **2006**, *118*, 6112–6116.
(22) Liu, J. J.; Galettis, P.; Farr, A.; Maharaj, L.; Samarasinha, H.; McGechan, A. C.; Baguley, B. C.; Bowen, R. J.; Berners-Price, S. J.; McKeage, M. J. In Vitro Antitumour and Hepatotoxicity Profiles of Au(I) and Ag(I) Bidentate Pyridyl Phosphine Complexes and Relationships to Cellular Uptake. *J. Inorg. Biochem.* **2008**, *102*, 303–310.
(23) Rackham, O.; Nichols, S. J.; Leedman, P. J.; Berners-Price, S. J.; Filipovska, A. A Gold(I) Phosphine Complex Selectively Induces Apoptosis in Breast Cancer Cells: Implications for Anticancer Therapeutics Targeted to Mitochondria. *Biochem. Pharmacol.* **2007**, *74*, 992–1002.
(24) Ott, I.; Scharwitz, M.; Scheffler, H.; Sheldrick, W. S.; Gust, R. Atomic Absorption Spectrometric Determination of the Iridium Content in Tumor Cells Exposed to an Iridium Metallodrug. *J. Pharm. Biomed. Anal.* **2008**, *47*, 938–942.
(25) Kirin, S. I.; Ott, I.; Gust, R.; Mier, W.; Weyhermüller, T.; Metzler-Nolte, N. Cellular Uptake Quantification of Metalated Peptide and Peptide Nucleic Acid Bioconjugates by Atomic Absorption Spectroscopy. *Angew. Chem., Int. Ed.* **2008**, *47*, 955–958.
(26) Sergeant, C. D.; Ott, I.; Sniady, A.; Meneni, S.; Gust, R.; Rheingold, A. L.; Dembinski, R. Metallo-nucleosides: Synthesis and Biological Evaluation of Hexacarbonyldicobalt 5-Alkynyl-2′-deoxyuridines. *Org. Biomol. Chem.* **2008**, *6*, 73–80.
(27) Marzano, C.; Gandin, V.; Folda, A.; Scutari, G.; Bindoli, A.; Rigobello, M. P. Inhibition of Thioredoxin Reductase by Auranofin Induces Apoptosis in Cisplatin-Resistant Human Ovarian Cancer Cells. *Free Radical Biol. Med.* **2007**, *42*, 872–881.
(28) Rigobello, M. P.; Messori, L.; Marcon, G.; Cinellu, M. A.; Bragadin, M.; Folda, A.; Scutari, G.; Bindoli, A. Mitochondrial Thioredoxin Reductase Inhibition by Gold(I) Compounds and Concurrent Stimulation of Permeability Transition and Release of Cytochrome C. *J. Inorg. Biochem* **2004**, *98*, 1634–1641.
(29) Rush, G. F.; Smith, P. F.; Hoke, G. D.; Alberts, D. W.; Snyder, R. M.; Mirabelli, C. K. The Mechanism of Acute Cytotoxicity of Triethylphosphine Gold(I) Complexes. II. Triethylphosphine Gold Chloride-induced Alterations in Mitochondrial Function. *Toxicol. Appl. Pharmacol.* **1987**, *90*, 391–400.
(30) Streicher, K. L.; Sylte, M. J.; Johnson, S. E.; Sordillo, L. M. Thioredoxin Reductase Regulates Angiogenesis by Increasing Endothelial Cell-Derived Vascular Endothelial Growth Factor. *Nutr. Cancer* **2004**, *50*, 221–231.
(31) Powis, G.; Kirkpatrick, D. L. Thioredoxin Signaling as a Target For Cancer Therapy. *Curr. Opin. Pharmacol.* **2007**, *7*, 392–397.
(32) Vacca, A.; Bruno, M.; Boccarelli, A.; Coluccia, M.; Ribatti, D.; Bergamo, A.; Garbisa, S.; Sartor, L.; Sava, G. Inhibition of Endothelial Cell Functions and of Angiogenesis by the Metastasis Inhibitor NAMI-A. *Br. J. Cancer* **2002**, *86*, 993–998.
(33) Ott, I.; Kircher, B.; Bagowski, C. P.; Vlecken, D. H. W.; Ott, E. B.; Will, J.; Bensdorf, K.; Sheldrick, W. S.; Gust, R. Modulation of the Biological Properties of Aspirin by Bioorganometallic Derivatisation. *Angew. Chem., Int. Ed.*, DOI: 10.1002/ange.200803347.
(34) Norrby, K. In Vivo Models of Angiogenesis. *J. Cell. Mol. Med.* **2006**, *10*, 588–612.
(35) Habeck, H.; Odenthal, J.; Walderich, B.; Maischein, H.; Schulte-Merker, S.; Tübingen 2000 Screen Consortium. Analysis of a Zebrafish VEGF Receptor Mutant Reveals Specific Disruption of Angiogenesis. *Curr. Biol.* **2002**, *12*, 1404–1412.
(36) Isenberg, J. S.; Jia, Y.; Field, L.; Ridnour, L. A.; Sparatore, A.; Del Soldato, P.; Sowers, A. L.; Yeh, G. C.; Moody, T. W.; Wink, D. A.; Ramchandran, R.; Roberts, D. D. Modulation of Angiogenesis by Dithiolethione Modified NSAIDs and Valproic Acid. *Br. J. Pharmacol.* **2007**, *151*, 142–151.
(37) Lawson, N. D.; Weinstein, B. M. In Vivo Imaging of Embryonic Vascular Development Using Transgenic Zebrafish. *Dev. Biol.* **2002**, *248*, 307–318.
(38) Ott, I.; Schmidt, K.; Kircher, B.; Schumacher, P.; Wiglenda, T.; Gust, R. Antitumor-Active Cobalt-Alkyne Complexes Derived from Acetylsalicylic Acid: Studies on the Mode of Drug Action. *J. Med. Chem.* **2005**, *48*, 622–629.
(39) Nicoletti, I.; Migliorati, G.; Pagliacci, M. G.; Grignani, F.; Riccardi, C. A Rapid and Simple Method for Measuring Thymocyte Apoptosis by Propidium Iodide Staining and Flow Cytometry. *J. Immunol. Methods* **1991**, *139*, 271–279.
(40) Riccardi, C.; Nicoletti, I. Analysis of Apoptosis by Propidium Iodide Staining and Flow Cytometry. *Nat. Protoc.* **2006**, *1*, 1458–1461.
(41) Fadok, V. A.; Xue, D.; Henson, P. If Phosphatidylserine Is the Death Knell, a New Phosphatidylserine-Specific Receptor Is the Bellringer. *Cell Death Differ.* **2001**, *8*, 582–587.
(42) Schlegel, R. A.; Williamson, P. Phosphatidylserine, a Death Knell. *Cell Death Differ.* **2001**, *8*, 551–563.
(43) Vermes, I.; Haanen, C.; Steffens-Nakken, H.; Reutellingsperger, C. A Novel Assay for Apoptosis. *J. Immunol. Methods* **1995**, *184*, 39–51.

JM8012135